Bull. Mater. Sci., Vol. 37, No. 3, May 2014, pp. 425–432. © Indian Academy of Sciences.

Nanocrystalline Pt-doped TiO_2 thin films prepared by spray pyrolysis for hydrogen gas detection

LALCHAND A PATIL*, DINESH N SURYAWANSHI, IDRIS G PATHAN and DHANASHRI G PATIL

Nanomaterials Research Lab, Department of Physics, Pratap College, Amalner 425 401, India

MS received 1 December 2012

Abstract. **Nanostructured pure and Pt-doped TiO_2 thin films were prepared by chemical spray pyrolysis technique. Aqueous solution of $TiCl_3 \cdot 6H_2O$ (0·01 M) was chosen as the starting solution for the preparation of pure TiO_2 thin film. Aqueous solutions of $PtCl_6 \cdot 6H_2O$ (0·01 M) and $TiCl_3 \cdot 6H_2O$ (0·01 M) were mixed in volume % of 1 : 99, 2·5 : 97·5 and 5 : 95 respectively to obtain Pt-doped TiO_2 thin films. The solutions were sprayed onto quartz substrate heated at 350 °C temperature to obtain the films. These thin films were fired for one hour at 550 °C. The sensing performance of these films was tested for various gases such as LPG, H_2, CO_2, ethanol, NH_3 and Cl_2 (1000 ppm). The Pt-doped TiO_2 (1 : 99) was observed to be most sensitive (572) to H_2 at 400 °C with high selectivity against other gases. Its response time was short (10 s) and recovery was also fast (14 s). To understand the reasons behind the gas-sensing performance of the films, their structural and microstructral properties were studied using X-ray diffraction and electron microscopy (FE–SEM and TEM), respectively. Thicknesses of all these samples were determined using Surface Profiler. The results are interpreted.**

Keywords. **Spray pyrolysis techniques; TiO_2 thin films; hydrogen gas response.**

1. Introduction

As hydrogen gas is tasteless, colorless and odorless, it cannot be detected by human beings. The low ignition energy and wide flammable range makes it easily inflammable and explosive. Therefore, rapid and accurate detection is necessary during the production, storage and use of hydrogen. It is also essential for monitoring/controlling the hydrogen concentration of nuclear reactors, coal mines and semiconductor manufacturing, etc. (Aroutiounian 2005; Buttner *et al* 2011; Hubert and Banach 2011). Various types of hydrogen sensors with different operating principles have been explored including the resistive type (Termick and Cavicchi 1991), thermoelectric (Matsumiya *et al* 2004), optical fibre (Okazaki *et al* 2003), surface acoustics wave (Jakubik *et al* 2003), carbon nanotube (Wong *et al* 2003) and cantilever-based sensors (Baselt *et al* 2003).

A few semiconducting metal oxides ZnO, SnO_2, Cr_2O_3 have been studied extensively for detection of toxic, hazardous and combustible gases (Wagh *et al* 2006; Bari *et al* 2009; Patil *et al* 2009, 2010, 2011). Recently, many efforts have been made to improve the gas sensor performances. Titanium dioxide is a very useful material and has been extensively investigated for its gas sensitive behaviour, excellent dielectric property as well as catalysis applications (Chen *et al* 2004; Ruiz *et al* 2004; Suryawanshi *et al* 2008).

In reactions involving titania, oxygen vacancies are one of the major advantages of such material. However, for better sensing performances, titania is doped with a variety of additives, such as platinum. These additives enhance the material sensitivity and selectivity and reduce the response time and operating temperature of the sensing layer. The application of nanomaterials to the design of hydrogen gas sensor is nowadays one of the most active research fields. This is due to their high activity, high surface-to-bulk ratio, good adsorption characteristics and high selectivity. The gas sensing mechanism involves chemisorptions of oxygen on the oxide surface, followed by charge transfer during the reaction between chemisorbed oxygen reducing and target gas molecules. However, the physical and sensing properties of semiconductor gas sensors are directly related to their preparation, e.g. particle size, sensing film morphology, crack surface (Ge *et al* 2007), and film thickness (Dayan and Phanichphant 1997; Sakai *et al* 2001; Zheng *et al* 2002; Liewhiran *et al* 2007) as well as sensing film characteristics.

In this article, we present the preparation and characterization of nanostructure pure and Pt-doped TiO_2 thin films and their gas-sensing properties. Nanostructure pure and Pt-doped TiO_2 thin films are prepared by spray pyrolysis deposition technique (SPD).

*Author for correspondence (plalachand _phy_aml @yahoo.co.in)

2. Experimental

2.1 *Experimental set-up to prepare nanostructured thin films*

Figure 1 shows a chemical spray pyrolysis technique for preparation of pure and Pt-doped TiO_2 nanocrystalline thin films. Set-up consists of spraying chamber, spray gun, air compressor, temp controller, and heater. Transparent, conducting, nonstoichiometric, nanocrystalline pure and Pt-doped TiO_2 thin films were prepared. The spray produced by nozzle was sprayed onto the glass substrates heated at 350 ± 10 °C. Various parameters such as nozzle-to-substrate distance, deposition time and flow rate of solution, deposition temperature and concentration were optimized to films in good quality.

2.2 *Preparation of TiO_2 thin films*

The spray pyrolysis technique was employed to prepare TiO_2 thin films. AR grade solution of $TiCl_3$ (0·01 M) was used as precursor. The solution was sprayed onto glass substrate heated at 350 °C to obtain the films. These thin films were fired for one hour at 550 °C and termed as S1.

2.3 *Preparation of Pt-doped TiO_2 thin films*

To prepare, platinum doped TiO_2 thin films, the solutions of AR grade $PtCl_6{\cdot}6H_2O$ (0·01 M) and titanium chloride ($TiCl_3$) (0·01 M) were mixed in the volume % (1: 99, 2·5: 97·5 and 5: 95). The solutions were sprayed on to glass substrate heated at 350 °C. These thin films were fired for one hour at 550 °C. Table 1 shows the preparative conditions of nanocrystalline TiO_2 thin films using spray pyrolysis.

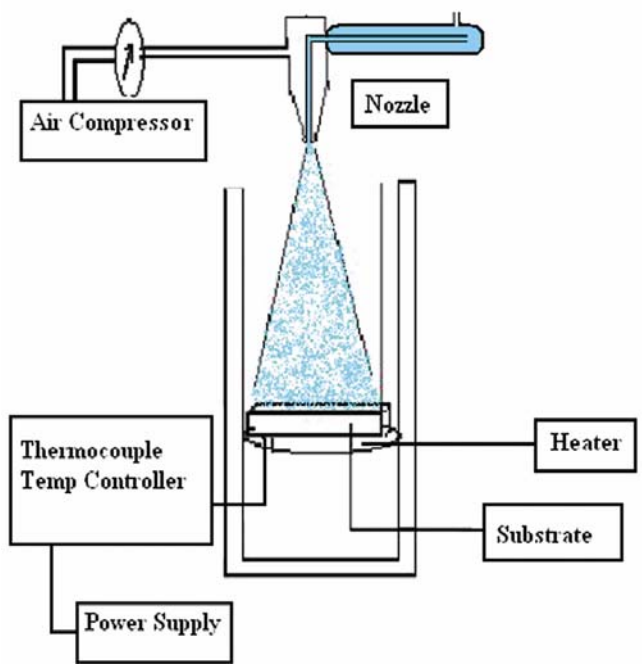

Figure 1. Spray pyrolysis system set-up.

2.4 *Thickness and roughness determination of thin films*

The thickness and roughness of thin films were measured by using surface profiler (AMBIOS Tech. (USA) XP-I) having a vertical resolution of 1·5 Å, lateral resolution of 100 nm and lateral length of 200 nm. The results are presented in table 2.

3. Material characterizations

As prepared nanostructured thin films were characterized by X-ray diffractometer using CuKα ($\lambda = 1{\cdot}5418$ Å) radiation. The quantitative elemental analyses of the films were estimated by JEOL-energy dispersive spectrometer (model JED-2300). TEM images were recorded from transmission electron microscope (CM 200 Philips (200 kV HT)). Thickness and roughness of thin films were measured by using surface profiler (AMBIOS Tech. (USA) XP-I). Electrical and gas sensing properties were measured using a static gas sensing system. The sensor performance on exposure of LPG, carbon dioxide, hydrogen, ammonia, ethanol and chlorine was examined.

3.1 *Crystal structure using X-ray diffraction*

Figure 2 represents the X-ray diffractograms of pure TiO_2 (S1) and Pt-doped TiO_2 (D1) thin films. The diffraction peaks from various planes and d-values are matching well with standard ASTM data, card no. 21-1272 of TiO_2. There are no prominent peaks of PtO associated in XRD pattern. It may be due to the smaller volume % of platinum doped in TiO_2. It reveals from XRD that the films are nanocrystalline in nature with anatase phase. All the peaks are corresponding to tetragonal TiO_2 with strongest (101) peak. The average crystallite size was calculated from (101) and (200) peaks, using Scherer formula and was found to be 12 nm for sample S1 and 18 nm for sample D1.

3.2 *Elemental composition of pure and Pt-doped TiO_2 thin films*

The quantitative elemental composition of pure TiO_2 and Pt-doped TiO_2 thin films were analyzed using an energy dispersive spectrometer and atomic % of O, Ti, Pt is represented in table 3. The samples are not perfectly stoichiometric, leading to semiconducting in nature (table 3).

Table 1. Preparation condition of TiO_2 and Pt-doped TiO_2 thin films.

Sample name	$PtCl_6$ (0·01 M) solution (mL)	$TiCl_3$ (0·01 M) solution (mL)	Substrate temp. (°C)	Firing temp. (°C)
S1	00·00	100·00	350	550
D1	01·00	99·00	350	550
D2	02·50	97·50	350	550
D3	05·00	95·00	350	550

Table 2. Thickness and roughness of pure and Pt-doped TiO_2 thin films.

Sample Number	Film thickness (nm)	Film roughness (nm)
S1	223·80	33·30
D1	21·10	05·50
D2	43·80	13·12
D3	57·20	15·50

Table 3. Elemental analysis of pure and Pt-doped TiO_2 thin films.

Element	Pure TiO_2 (S1)	Pt-doped TiO_2 (D1)	Pt-doped TiO_2 (D2)
O	71·73	86·70	87·44
Ti	28·27	12·29	10·90
Pt	00·00	01·01	01·66
Total	100·00	100·00	100·00

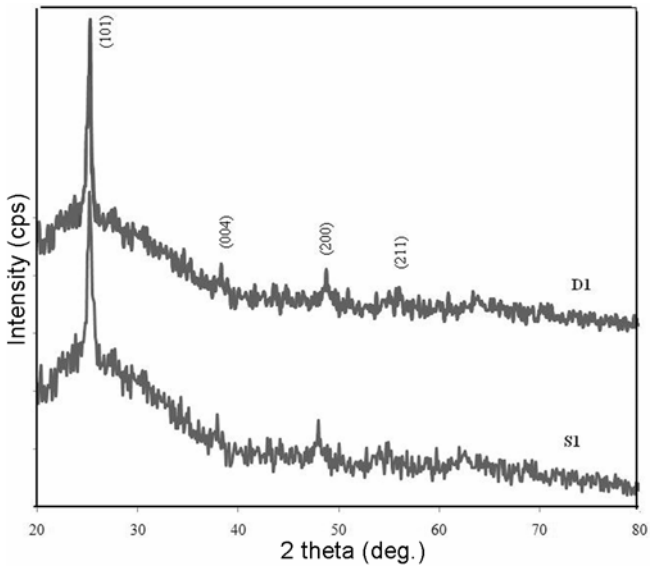

Figure 2. XRD of pure (S1) and Pt-doped TiO_2 (D1) thin films.

3.3 *Surface morphology of pure TiO_2 thin film*

Figure 3 depicts the FE–SEM of sample S1 fired at 550 °C for 60 min. Pure TiO_2 thin film is observed to be continuous, dense and without any cracks and it consists of uniformly distributed grains having average crystallite size of 13 nm. The histogram shows grain size distribution in sample S1.

3.4 *Surface morphology Pt-doped TiO_2 thin film*

Figures 4(a) and (b) show surface morphology of D1 and D2 thin films, respectively. The histograms 4(c) and 4(d) show the grain size distribution in D1 and D2 samples. The grains of D1 are ellipsoidal in nature with an average grain size of 27 nm and D2 film consists of grains with an average grain size of 36 nm. It is clear from figures 4(a) and (b) that some very small white particles are dispersed uniformly on the surface of both D1 and D2 films. The numbers of such particles are observed to be increasing with increase in Pt-doping concentration. These particles may be of platinum.

3.5 *Transmission electron microscopy of pure and Pt-doped TiO_2 thin films*

Figure 5(a) and (c) show the transmission electron microscopy (CM 200 Philips (200 kV HT)) of powders obtained by scratching the thin films of sample S1 and sample D1. The powder was dispersed in ethanol. Transmission microscopy uses copper grid to hold the powder. It is clear from TEM images that the grains are spherical in shape and nanocrystalline in nature with average crystallite size of 10·52 nm in case of S1 and 16·21 nm in case of D1. Additional structural characterization was carried out by electron diffraction shown in figures 5(b) and (d). Spherical rings in electron diffraction patterns suggest that the nanopowders have good crystallinity. The images show the clear fringes corresponding to the (101), (004), (200), (211), (204) and (116) lattice planes of TiO_2. It is clear from TEM images that there are nanocrystallites in the powders and turn in the films. The average crystalline size observed from XRD and grain size from TEM and FESEM are listed in table 4.

4. Electrical properties of the sensor

4.1 *I–V characteristics*

Figure 6 shows *I–V* characteristics of nanostructured pure and Pt-doped TiO_2 thin films. The graphs are observed to be symmetrical in nature indicating ohmic contact.

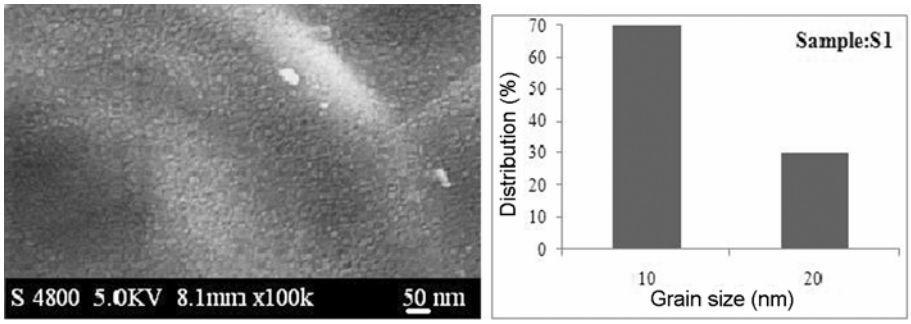

Figure 3. FE–SEM image with histogram: sample S1.

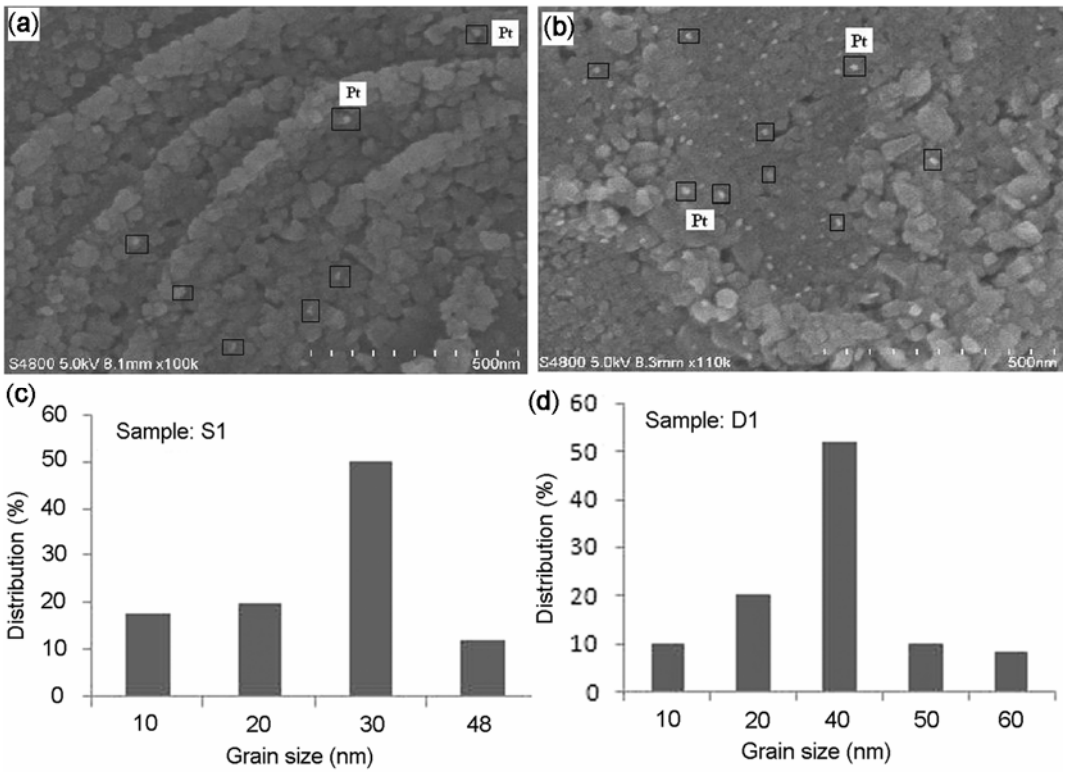

Figure 4. FE–SEM images with histograms: sample D1 (**a**, **c**), sample D2 (**b**, **d**).

4.2 *Electrical conductivity*

Figure 7 shows the variation in electrical conductivity of thin film samples S1, D1, D2 and D3 with temperature. Electrical conductivity measurement for each film was made in the temperature range between 250 and 450 °C in steps of 50 °C. It is clear from the graphs that electrical conductivity goes on increasing with temperature for all samples.

4.3 *Gas-sensing performance of the sensor*

The gas-sensing performance of the nanostructured thin films was tested using static gas-sensing system explained elsewhere (Jain *et al* 2006).

4.4 *Sensing performance of pure TiO_2 thin films*

Figure 8 shows the variation of gas (1000 ppm) responses of pure TiO_2 thin film. The pure TiO_2 thin film showed highest response to LPG at 350 °C (24) and H_2 at 250 °C (27). The same sensor responded to LPG and hydrogen, respectively at 350 and 250 °C. Therefore, pure TiO_2 thin film showed temperature dependent sensing properties.

4.5 *Sensing performance of Pt-doped TiO_2 thin films*

Figure 9 shows variation in hydrogen response with operating temperature. It is clear from the figure that the gas response increases with operating temperature, reaches

Table 4. Measurement of crystalline and grain size.

	Average crystalline size	Average grain size	
Sample name	XRD (nm)	TEM (nm)	FESEM (nm)
S1	12	10·52	13
D1	18	16·21	27

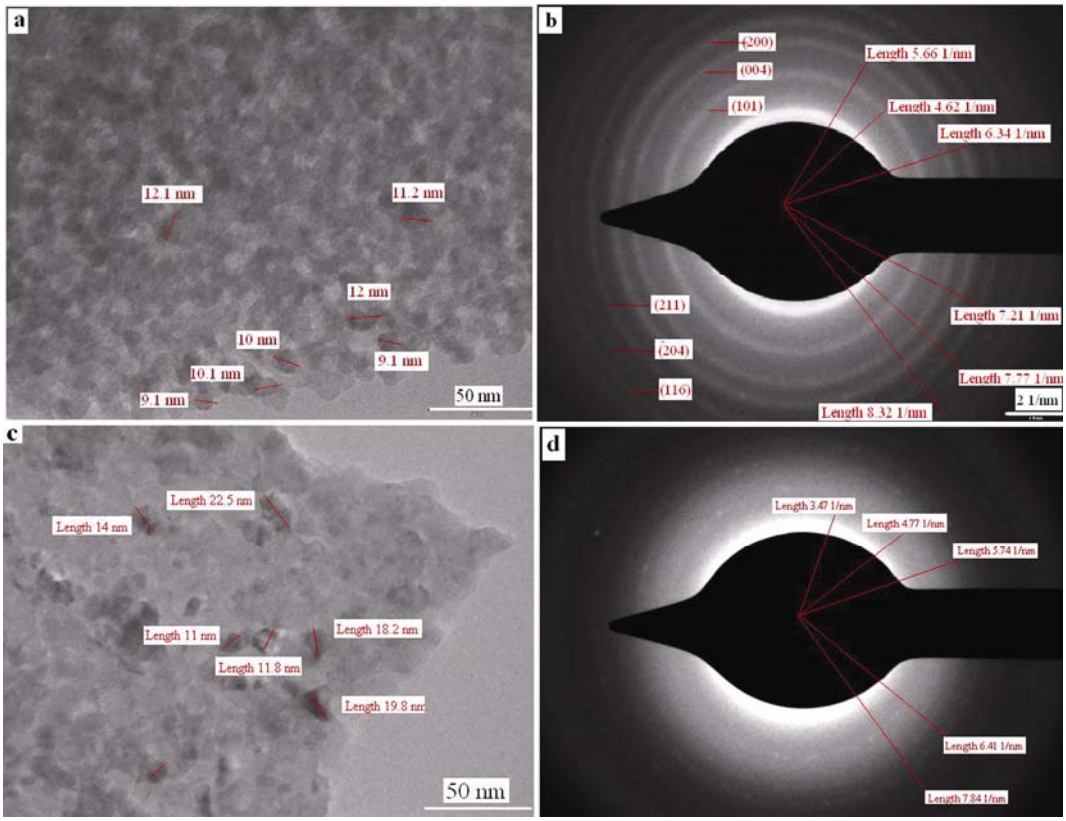

Figure 5. TEM and electron diffraction images: sample S1 (**a**, **b**) and sample D1 (**c**, **d**).

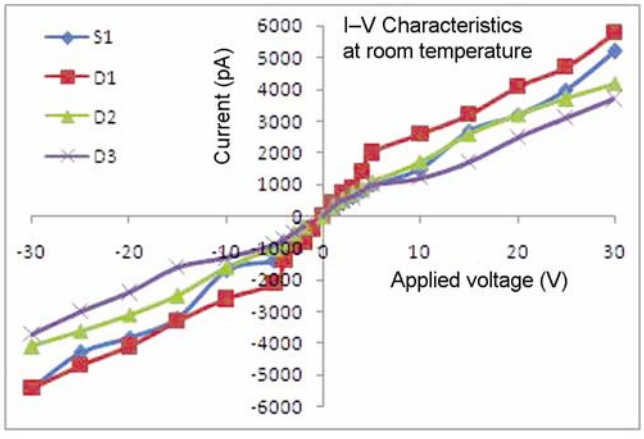

Figure 6. *I–V* characteristics of Pt-doped TiO_2 thin films.

maximum ($S = 578$) at 400 °C and then falls with further increase in operating temperature. Higher sensitivity of Pt-doped TiO_2 (D1) may be due to spill over action of platinum and nanocrystalline nature of film (16·21 nm). High surface to volume ratio (available due to nanocrystalline nature) allows gas to interact with larger surface area giving ultra large gas response (Young *et al* 1987).

Table 1 shows the thickness of sample D1 as 21·10 nm which is very small as compared to sample D2 and D3. It is clear from the reported data (Jin *et al* 1998; De *et al* 1999; Hammond and Liu 2001) that the gas sensitivity of nanocrystalline thin film increases with decreasing film thickness (Shukla and Seal 2003). The increase in the gas sensitivity with decrease in the film thickness can be explained on the basis of the model proposed by (Sakai *et al*).

4.6 *Selectivity*

Sensing performances of the Pt-doped TiO_2 thin films (D1, D2, D3) were tested by exposing them with Ethanol, CO_2, Cl_2, LPG, H_2 and NH_3 gases.

Figure 10 shows selectivity of nanostructured Pt-doped TiO_2 thin films to H_2 against CO_2, LPG, NH_3, Cl_2 and

ethanol gases at 400 °C. It is clear from the figure that the nanostructured Pt-doped TiO_2 thin films were found to be highly selective to H_2 at 400 °C against other gases.

4.7 *Response and recovery of sensor*

The time taken for the sensor to attain 90% of the maximum decrease in resistance on exposure to the target gas, is the response time. The time taken for the sensor to get back 90% of original resistance is the recovery time. The response and recovery of sensor (D1), on exposure of 1000 ppm of H_2 at 400 °C, are represented in figure 11. The response time of the sensor was observed to be (10 s) and the recovery time was (14 s). Sensor showed quick response and fast recovery.

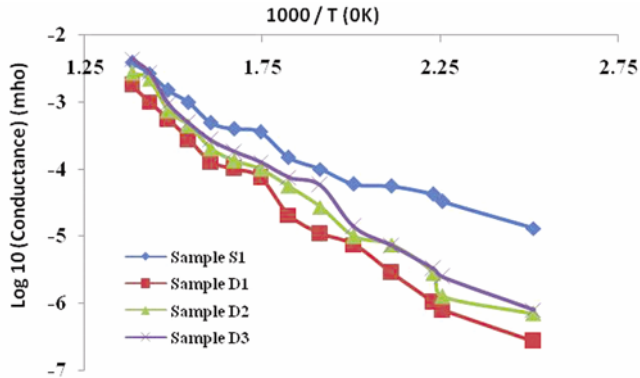

Figure 7. Conductivity–temperature profile.

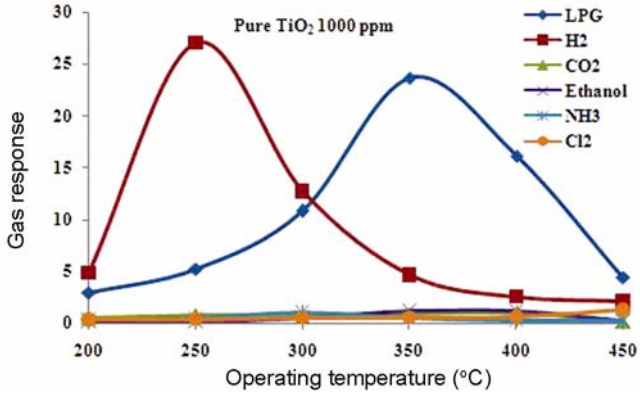

Figure 8. Variation of gas response with operating temperature.

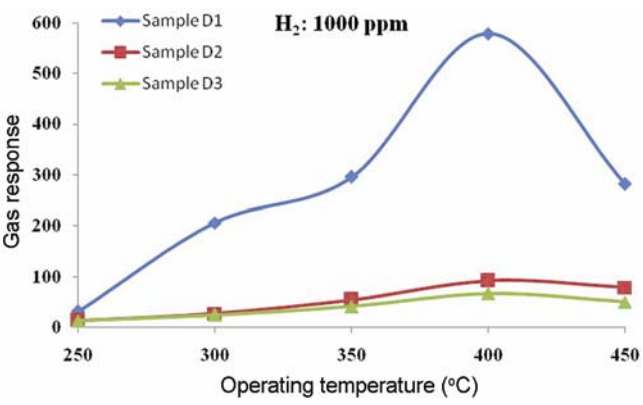

Figure 9. H_2 gas response–operating temperature profile.

5. Discussion

The most important features of the present investigation are: high gas response, high selectivity to hydrogen against other gases, fast response and quick recovery. The enhanced response could be attributed to nanocrystalline nature of the films. It is known that, when nanocrystalline Pt-doped TiO_2 semiconductor thin film is exposed to air, physisorbed oxygen molecules pick up electrons from the conduction band of Pt–TiO_2 and change to O^-_{2ads} or O^-_{ads} species (Morrison *et al* 2001) as indicated in (1) and (2):

$$O_2\,(\text{gas}) + e^- \rightarrow O_2\,(\text{ads})^-, \quad (1)$$

$$O_2\,(\text{ads})^- + e^- \rightarrow 2O\,(\text{ads})^-. \quad (2)$$

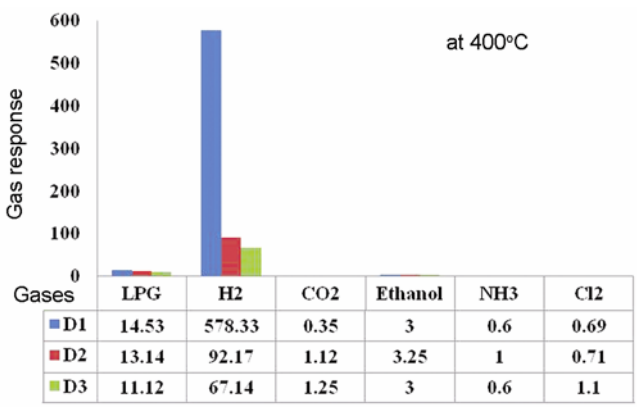

Gases	LPG	H2	CO2	Ethanol	NH3	Cl2
D1	14.53	578.33	0.35	3	0.6	0.69
D2	13.14	92.17	1.12	3.25	1	0.71
D3	11.12	67.14	1.25	3	0.6	1.1

Figure 10. Response of sensor to various gases (selectivity).

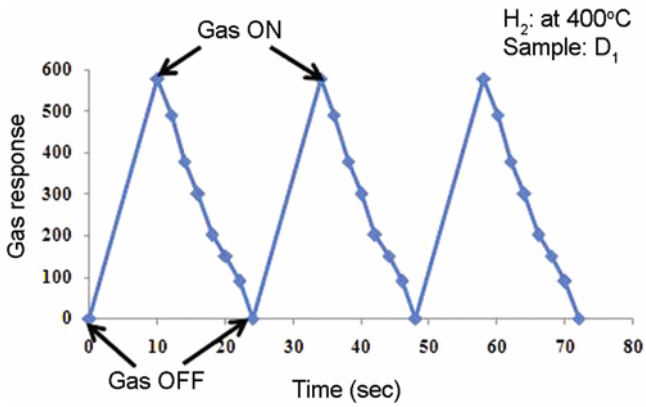

Figure 11. Response and recovery of sensor.

The adsorption of O_2^- and O^- ions on the nanocrystalline Pt-doped TiO_2 surface is vital to enhance the receptor function of the sensor and, hence, its gas response. The receptor function is an ability of metal oxide surface to receive the target gas, which is directly related to surface capability to adsorb O_2^- and O^- ions. Larger the ability of the surface to receive and oxidize the target gas, larger could be the change in conductivity of the sensor and, hence, enhancement in gas response. Number of O_2^- and O^- ions adsorbed on the surface also depends on oxygen-ion vacancies within the Pt-doped TiO_2 lattice. Oxygen-ion vacancies, within the Pt-doped TiO_2 lattice, can result in increased adsorption of the oxygen-ions (O_2^- and O^- ions) on the sensor surface. Any mechanism that can increase the lattice oxygen-ion vacancy concentration can lead to significant increase in both the receptor function and the gas response of the nanocrystalline Pt-doped TiO_2 sensors.

The interaction between adsorbed O_2^- and O^- ions (on the Pt–TiO_2 surface) and hydrogen, target gas, can be explained in terms of reactions (3) and (4) as follows:

$$2H_2 + O_2^- (ads) = 2H_2O + e^-, \quad (3)$$

or

$$H_2 + O^- (ads) = H_2O + e^-. \quad (4)$$

In addition, the usage of nanostructures increases the surface to volume ratio which generally enhances the sensor response. The increase in the surface area of nanostructured materials can also lead to increase in catalytic activity or surface adsorption.

It is widely believed that Pt-catalyst enhances reducing gas sensing of metal oxide via spillover mechanism (Morrison 1982). This interaction is a chemical reaction by which additives assist the redox process of metal oxides. The term 'spill over' refers to the process, illustrated in figure 12. In this process, the metal catalyst dissociates from the molecule and then the atom can 'spill over' onto the surface of the semiconductor support. At appropriate temperatures, reactants are first adsorbed on to the surface of additive particles and then migrate to the oxide surface to react there with surface oxygen species, affecting the surface conductivity. For the above processes to dominate the metal oxide resistance, the spilled-over species must be able to migrate to the interparticle contact. Thus, for a catalyst to be effective, there must be a good dispersion of the catalyst so that catalyst particles are available near all contacts. Only then can the catalyst affect the important interparticle contact resistance.

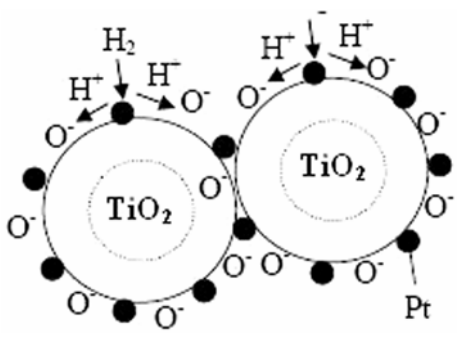

Figure 12. Gas sensing mechanisms based on 'spill over' effect of Pt-doped TiO_2 nanoparticles.

6. Conclusions

Chemical spray pyrolysis technique is simple, convenient, and 'green': it may be used to large scale industrial application for preparation of nanostructured metal oxides. Because the nanostructured thin films and nanoparticles have large surface area, stable structure, and a particular inner environment, such materials may find great applications in gas sensing, heterogeneous catalysis, optical devices, and micro reactors. Very high resistance before exposure of target gas and very low resistance in presence of target gas are the most important characteristics of nanocrystalline Pt-doped TiO_2 thin films. Pure TiO_2 thin film shows maximum gas response to H_2 (27). Addition of Pt was observed to enhance sensitivity (572) and selectivity to H_2 gas. Response and selectivity of the Pt-doped TiO_2 thin film to hydrogen gas were observed to be extremely high in comparison to NH_3, CO_2, Cl_2, LPG and C_2H_5OH. The enhanced gas response could be attributed to nanocrystalline nature of the films. Hydrogen gas response of the present nanocrystalline Pt-doped TiO_2 thin film sensor may be due to the simultaneous activation of its receptor (due to the adsorption of O_2^- and O^- ions on the surface) and transducer (due to the 'grain control' resistance mechanism) functions.

References

Ansari S G, Boroojerdain P, Sainkar S R, Karekar R N, Aiyer R C and Kulkarni S K 1997 *Thin Solid Films* **295** 271

Aroutiounian V 2005 *Int. Sci. J. Altern. Energy Ecol.* **3** 21

Babari F H and Orvatinia M 2003 *Sensors & Actuators* **B89** 256

Baik N S, Miura N and Yamazoe N 2001 *Sensors & Actuators* **B77** 116

Bari A R, Shinde M D, Deo V and Patil L A 2009 *Indian J. Pure Appl. Phys.* **47** 24

Baselt D R, Fruhberger B, Klaassen E, Cemalovic S, Brittion C L Jr, Patel S V, Mlsna T E, McCorkle D and Warmack B 2003 *Sensors & Actuators* **B88** 120

Buttner W J, Post M B, Burgess R and Rivkin C 2011 *Int. J. Hydrogen Energy* **36** 2462

Chang J F, Kuo H H, Leu I C and Hon M H 2002 *Sensors & Actuators* **B84** 258

Chen W, Fang Q, Li S, Wu J, Li F and Jiang K 2004 *Sensors & Actuators* **B100** 195

Christoulakis S, Suchea M, Koudoumas E, Katharakis M and Katsarakis N 2006 *Appl. S* 5351

Dayan N J, Karekar R N, Aiyer R C and Sainkar S R 1997 *J. Mater. Sci.-Mater. Electron.* **8** 277
Devi G S, Hyodo T, Shimizu Y and Egashira M 2002 *Sensors and Actuators* S*urf. Science* **B87** 252
Ge D, Xie C and Cai S 2007 *Mater. Sci. Eng.* **B13** 753
Geistlinger H 1993 *Sensors & Actuators* **B17** 47
Hammond J W and Liu C C 2001 *Sensors & Actuators* **B81** 25
Hubert and Banach L G 2011 *Sensors & Actuators* **B157** 329
Jain G H, Patil LA, Wagh M S, Patil D R, Patil S A and Amalnerkar D P 2006 *Sensors & Actuators* **B117** 159
Jakubik W P, Urbanczyk M W, Kochowski S and Bodzenta J 2003 *Sensors & Actuators* **B96** 321
Jin Z, Zhou H -J, Jin Z -L, Savinell R F and Liu C -C 1998 *Sensors & Actuators* **B52** 188
Jun, Youn-Ki Kim, Hyun-Su, Lee Jong-Heun and Hong Seong-Hyeon 2005 *Sensors & Actuators* **B107** 264
Lee Y L, Sheu C Y and Hsiao R H 2004 *Sensors & Actuators* **B99** 281
Liewhiran C and Phanichphant S 2007 *Sensors* **7** 185
López M A, Peiteado R, Fernandez M, Caballero J F, Holc A C, Drnovsek J, Kuscer S, Macek D and Kosec S 2006 *J. Eur.* **26** 2985
Matsumiya M, Qiu F, Izu N and Murayama N 2004 *Sensors & Actuators* **B97** 344
Morrison S R 1982 Sensors *& Actuators* **B2** 329
More P S, Karekar R N, Bhoraskar S V, Sai N D and Aiyer R C 2004 *Mater. Lett.* **58** 1020
Okazaki S, Nakagawa H, Asakura S, Tomiuchi Y, Tsuji N, Murayama H and Washiya M 2003 *Sensors & Actuators* **B93** 142
Okuya M, Nakade K D, Osa T, Nakano, Kumara and Shoji Kaneko 2004 *J. Photochem. Photobiol. A Chemistry* **164** 167
Patil D R and Patil L A 2007 *Sensors & Transducers* **81** 1354
Patil L A, Shinde M D, Bari A R and Deo V V 2009 *Sensors and Actuators* **B143** 316
Patil L A 2009 *Sensors and Transducer* **104** 68
Patil L A, Shinde M D, Bari A R and Deo V 2009 *Sensors & Actuators* **B143** 270
Patil L A, Shinde M D, Bari A R and Deo V V 2010 *Curr. Appl. Phys.* **10** 1249
Patil L A, Shinde M D, Bari A R and Deo V V 2011 *Mater. Sci. Eng.* **B176** 579
Patil S A, Patil L A, Patil D R, Jain G H and Wagh M S 2007 *Sensors & Actuators* **B123** 233
Quaranta F, Rella R, Sicilian P, Capone S, Epifani M, Vasanelli L, Licciulli A and Zocco A 1999 *Sensors & Actuators* **B58** 350
Rella R, Serra A, Siciliano P, Vasanelli L, De, Licciulli and Quirini A 1997 *Sensors & Actuators* **B44** 462
Ruiz A M, Cornet A and Morante J R 2004 *Sensors & Actuators* **B100** 256
Shimizu Y, Kuwano N, Hyodo T and Egashira M 2002 *Sensors & Actuators* **B83** 195
Shukla S and Seal S 2003 *Encyclopedia of nanoscience and nanotechnology* (Stevenson Ranc: American Scientific Publishers)
Suryawanshi D N, Patil D R and Patil L A 2008 *Sensors & Actuators* **B134** 579
Termick and Cavicchi R E 1991 *Thin Solid Films* **206** 81
Thomas I L 2001 *Nanoscience* **4** 332
Wagh M S, Jain G H, Patil D R, Patil S A and Patil L A 2006 *Sensors & Actuators* **B115** 128
Wong Y M, Kang W P, Davidson J L, Wisitsora-a A and Soh K L 2003 *Sensors & Actuators* **B93** 327
Young V Y, Chang F C and Cheng K L 1987 *Appl. Spectrospy* **41** 994
Zheng L, Xu T, Li G and Yin Q 2002 *Jpn. J. Appl. Phys.* **41** 4655